Simplified model of cytosolic Ca^{2+} dynamics in the presence of one or several clusters of Ca^{2+}-release channels

G. Solovey,[1] D. Fraiman,[2] B. Pando,[3] and S. Ponce Dawson[1]
[1]*Departamento de Física, FCEN-UBA, Ciudad Universitaria, Pabellón I, (1428) Buenos Aires, Argentina*
[2]*Departamento de Matemática y Ciencias, Universidad de San Andrés, Buenos Aires, Argentina*
[3]*Department of Physics, Massachusetts Institute of Technology, Cambridge, Massachusetts 02139, USA*
(Received 22 April 2008; published 23 October 2008)

Calcium release from intracellular stores plays a key role in the regulation of a variety of cellular activities. In various cell types this release occurs through inositol-triphosphate (IP_3) receptors which are Ca^{2+} channels whose open probability is modulated by the cytosolic Ca^{2+} concentration itself. Thus, the combination of Ca^{2+} release and Ca^{2+} diffusion evokes a variety of Ca^{2+} signals depending on the number and relative location of the channels that participate of them. In fact, a hierarchy of Ca^{2+} signals has been observed in *Xenopus laevis* oocytes, ranging from very localized events (puffs and blips) to waves that propagate throughout the cell. In this cell type channels are organized in clusters. The behavior of individual channels within a cluster cannot be resolved with current optical techniques. Therefore, a combination of experiments and mathematical modeling is unavoidable to understand these signals. However, the numerical simulation of a detailed mathematical model of the problem is very hard given the large range of spatial and temporal scales that must be covered. In this paper we present an alternative model in which the cluster region is modeled using a relatively fine grid but where several approximations are made to compute the cytosolic Ca^{2+} concentration ($[Ca^{2+}]$) distribution. The inner-cluster $[Ca^{2+}]$ distribution is used to determine the openings and closings of the channels of the cluster. The spatiotemporal $[Ca^{2+}]$ distribution outside the cluster is determined using a coarser grid in which each (active) cluster is represented by a point source whose current is proportional to the number of open channels determined before. A full reaction-diffusion system is solved on this coarser grid.

DOI: 10.1103/PhysRevE.78.041915 PACS number(s): 87.17.−d, 82.33.−z, 02.30.Jr, 87.16.Vy

I. INTRODUCTION

The calcium ion (Ca^{2+}) is a universal second messenger that is involved in the regulation of a large number of physiological processes [1]. To attain this difficult task, the cytosolic Ca^{2+} concentration ($[Ca^{2+}]$) is precisely regulated. One of the channels that regulates intracellular calcium is the inositol 1,4,5-trisphosphate (IP_3) receptor (IP_3R) which is expressed in many cell types and is located at the surface of intracellular membranes such as the endoplasmic reticulum (ER), the sarcoplasmic reticulum (SR), and the nucleus. The IP_3R is biphasically regulated by Ca^{2+}, with a bell-shaped open probability as a function of $[Ca^{2+}]$. This leads to a phenomenon called Ca^{2+}-induced Ca^{2+} release (CICR) because the Ca^{2+} ions released by one channel can in turn trigger the opening of another nearby channel.

The *Xenopus laevis* oocyte is a useful system to study intracellular Ca^{2+} signals because of its large size and because the only Ca^{2+} channels that are present at the surface of the ER are IP_3R's. In oocytes, IP_3R's are organized in clusters of width ~100 nm [2–4] that are separated by a few micrometers [5]. As a result of the combination of CICR and this spatial organization [6–8], cytosolic Ca^{2+} signals in oocytes display a hierarchical spatiotemporal organization, which includes Ca^{2+} "blips" that represent the release of Ca^{2+} through a single IP_3R [9–11], "puffs" that involve the concerted opening of several IP_3R's in a cluster [10–13], and Ca^{2+} waves that propagate globally across cells by successive cycles of CICR and Ca^{2+} diffusion between clusters [12–14]. The whole range of signals has been observed using fluorescence microscopy and Ca^{2+} sensitive dyes.

Fluorescence microscopy techniques allow the visualization of Ca^{2+} signals and, at the same time, provide a means by which the dynamics of IP_3R's can be studied under more physiological conditions than with other methods. Nevertheless, since the spatial resolution of fluorescent images is usually of hundreds of nanometers, it is impossible to resolve the $[Ca^{2+}]$ spatiotemporal distribution within the cluster region or to study the dynamics of single IP_3R's. The use of mathematical models that span the scale that goes from single channel pores ($\leqslant$10 nm [15]) to inter-cluster distances (~2 μm [5]) is thus unavoidable in order to obtain a detailed description of Ca^{2+} puffs. Furthermore, these models provide a framework within which one can test hypothetical models of single IP_3R's. In fact, there is a large body of experimental and modeling results on single IP_3R's [16–20] and it is important to advance towards a comprehensive description that combines this variety of observations in a unified way. The use of mathematical models is unavoidable for this purpose too. On the other hand, a unified description of all the repertoire of Ca^{2+} signals that have been observed requires that the mm scale be also included. This diversity of spatial (and temporal) scales represents a challenge to theoretical approaches. The numerical simulation of the reaction-diffusion systems that are usually used to model the cytosolic Ca^{2+} dynamics is a very stiff (and computationally expensive) problem. For this reason, several simplified models and theoretical approaches have been proposed to analyze different aspects of Ca^{2+} signals.

The simplest signal that can be studied is the one that arises due to the opening of a single Ca^{2+} channel. The analysis of the $[Ca^{2+}]$ distribution in the presence of a single

source is actually the first step of our work. Several studies have used approximations of the complete reaction-diffusion problem to find analytical expressions for the $[Ca^{2+}]$ close to the open channel. These results were put in a rigorous basis and extended in [21]. More recently, Bentele and Falcke [22] have exploited the fast time scales of the local concentrations build up to find analytical expressions for the current and $[Ca^{2+}]$ close to the open channel. Shuai and Parker [23] also simulated microdomains of Ca^{2+} ions and Ca^{2+}-bound indicator dye around an open channel in order to understand the processes that determine the temporal resolution and the noise level of single-channel Ca^{2+} fluorescence signals (SCCaFTs).

Other signals involve the release of Ca^{2+} from several open channels in a cluster. The dynamics of clusters of IP_3R's has been studied with a variety of approaches which focus on different properties depending on the spatial and time scale that they resolve. One type of model, called "fire-diffuse-fire," introduced to study $[Ca^{2+}]$ waves, simplify clusters by considering them as discrete excitable Ca^{2+} release elements that open when a certain threshold amount of Ca^{2+} is achieved [24]. This model is useful to understand general properties of wave propagation, such as the transition between saltatory and continuous propagation, based on simple physical ideas, but does not take the internal structure and complexity of the clusters into account. Several mathematical models have been proposed to describe Ca^{2+} release through clustered IP_3R's and some of them rely on the hypothesis that channels are in such close contact that $[Ca^{2+}]$ can be considered homogeneous throughout the cluster [25–30]. This assumption allows for relatively fast simulations of cytosolic Ca^{2+} dynamics since Ca^{2+} diffusion within the cluster can be neglected. This type of models can be further simplified as done in Ref. [31,32], where it is assumed that $[Ca^{2+}]$ at one cluster depends only on the number of nearest release sites where there are open channels and that each neighboring (active) site adds a time-independent contribution to $[Ca^{2+}]$. In the case of only one cluster the system is spherically symmetric, which further reduces the computational effort. In this case the cluster can be considered as a localized point source with a Ca^{2+} current that depends on the number of open channels. However, if one is willing to include a more accurate description of the Ca^{2+}-release process kinetics, which depends on the time at which each channel of the cluster becomes open, it is necessary to have a better estimate of the $[Ca^{2+}]$ value at each channel pore within the cluster. Namely, the Ca^{2+} concentration nearby an open Ca^{2+} channel has a sharp spatial decay [18,21,23,33,34], so even at interchannel distances ($\sim$tens of nm), the $[Ca^{2+}]$ gradient is so high that neglecting its inhomogeneities may not be a good approximation. The existence of these deep gradients that usually build up very fast impose a serious difficulty to quantitative modeling approaches. Keeping the same spatial resolution both inside and outside the cluster is computationally expensive [2,18,35]. One alternative is to use a spatial grid that is finer inside than outside the clusters. However, finer spatial grids usually call for smaller time steps and, therefore, longer computation times. Another option is to use a finite element method to resolve the extreme spatial gradients of concentration values close to the channel. This method was applied in Ref. [35] to study Ca^{2+} "blips." In their work, the authors introduce an hybrid algorithm to reliably link the stochastic transitions of the state of the channel with the deterministic concentration variables. So far this method has been applied to single channel simulations [35], where it has shown its accuracy compared to standard methods.

In this work we present an alternative model in which a fine grid is used to determine the $[Ca^{2+}]$ concentration distribution within the cluster but its dynamics is described within a quasistationary approximation. In order to determine the contribution of each open channel to the $[Ca^{2+}]$ distribution within the cluster, we analyze first this distribution when there is only one channel in the presence of the same amount of buffers as in the full scenario. The total $[Ca^{2+}]$ within the cluster when there are several open channels is then approximated by a linear combination of the contributions due to each individual open channel. This detailed description of $[Ca^{2+}]$ within the cluster is used to determine the openings and closings of the various channels in each release site. In this way we obtain the total Ca^{2+} current that is released from any given cluster. The spatiotemporal $[Ca^{2+}]$ distribution outside the cluster is determined using a coarser grid in which each (active) cluster is represented by a point source whose current is proportional to the number of open channels determined before. A full reaction-diffusion system is solved on this coarser grid.

This model allows us to obtain the distribution of Ca^{2+} in the presence of clusters of IP_3R's in a much shorter time than the one required to solve a complete system of reaction-diffusion equations on a very fine grid. The Ca^{2+}-bound dye distribution, a quantity that is directly related to the fluorescence distribution observed experimentally, is readily determined with the model. This simplified solution describes correctly global Ca^{2+} signals with the spatial resolution of experiments using the stochastic single channel activity as a building block.

The organization of the paper is as follows. We first introduce the (full) reaction-diffusion model that describes the dynamics of intracellular Ca^{2+} for the problem of interest (Sec. II). In Sec. III we first study the solutions of this model in the presence of a single localized source. We then analyze to what extent this single channel solution can be used to determine the $[Ca^{2+}]$ distribution within the cluster region when there are several open channels. We approximate the numerically determined solution in various ways and analyze the validity of the approximations in a number of particular examples. In Sec. IV we show that the $[Ca^{2+}]$ spatiotemporal distribution outside the cluster region can be determined using the full reaction-diffusion model on a grid that is coarser than the cluster size. We show that, on this coarser grid, each cluster can be represented by a point source whose total current is equal to the one determined within the cluster region. In Sec. V we put everything together to show in a step by step manner how to build a complete description of Ca^{2+} dynamics resulting from an isolated puff. In Sec. VI we generalize the model to the case of multiple clusters and show that it is able to reproduce efficiently Ca^{2+} signals that propagate throughout the cell. Finally, we include a final discussion with conclusions in Sec. VII.

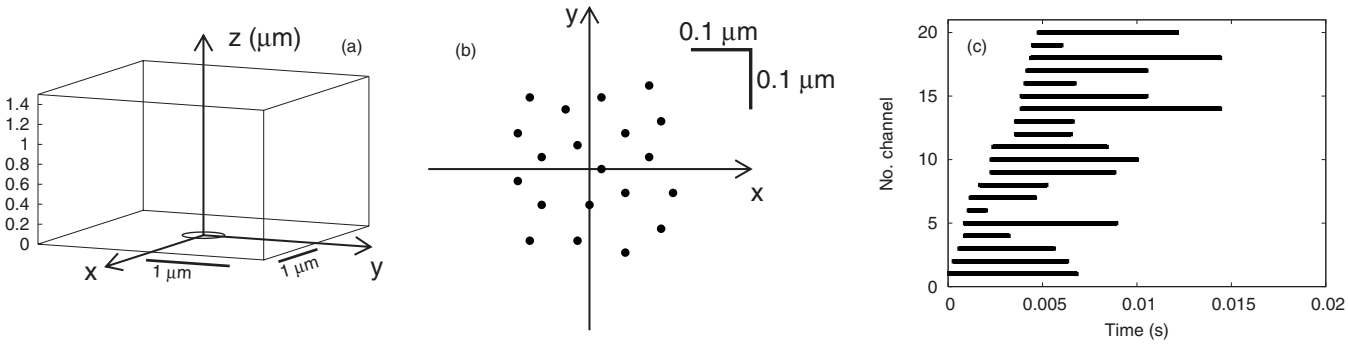

FIG. 1. (a): Geometry of the cytosolic space. The illustration corresponds to a situation with one cluster of IP_3R's centered around the origin, $\mathbf{r}=\mathbf{0}$ and when individual IP_3R's are considered as the Ca^{2+} sources. The plane $z=0$ represents the surface of the ER. (b) A detailed view of a cluster of $N_s=20$ channels randomly distributed within a region of 300×300 nm at the surface of the ER. (c) A graphical representation of the open and close time of each of the N_s channels. The length of the black lines indicate the time interval during which the channels remain open. In this case the behavior of the channels was fixed *a priori* by setting the open and closed time for each of them.

II. FULL MATHEMATICAL MODEL OF CYTOSOLIC CALCIUM DYNAMICS IN THE PRESENCE OF LOCALIZED CALCIUM SOURCES

We present here a model of Ca^{2+} diffusion in a cytosolic medium with molecular buffers and localized Ca^{2+} sources. The model is a standard reaction diffusion scheme, similar to others that have been introduced previously [2,8,23,30,35]. It includes the following species: cytosolic calcium (Ca^{2+}), an immobile endogenous buffer (S), a cytosolic Ca^{2+} indicator (Fluo4) and an exogenous mobile buffer (EGTA, or BAPTA). The Ca^{2+} indicator represents the dye usually used in fluorescent microscopy experiments [36,37]. Exogenous buffers are used in experiments to prevent the initiation of Ca^{2+} waves [36,37]. The equations we derive in this section are the same whether we use BAPTA or EGTA (only some parameter values change). In the following, we use EGTA except explicitly noted. We consider that a single Ca^{2+} ion can bind to a single buffer or dye molecule according to

$$Ca^{2+} + X \underset{k_{\text{off}}^X}{\overset{k_{\text{on}}^X}{\rightleftharpoons}} CaX, \tag{1}$$

where X represents S, EGTA or Fluo, and k_{on}^X and k_{off}^X are the forward and backward binding rate constants of the corresponding reaction, respectively. We assume that the total concentration of Ca^{2+} indicator, mobile and immobile buffer remain constant ($[\text{Fluo}]_T$, $[\text{EGTA}]_T$, and $[S]_T$, respectively) and that the diffusion coefficient of their free and Ca^{2+}-bound forms are equal. Therefore, we can calculate [Fluo], [S], and [EGTA] by subtracting the concentration of the Ca^{2+} bound forms to the total concentration. Given these assumptions, the set of partial differential equations that give the spatial and temporal evolution of free and bound Ca^{2+} is the following:

$$\frac{\partial[Ca^{2+}]}{\partial t} = D_{Ca^{2+}}\nabla^2[Ca^{2+}] - \sum_X R_{CaX}, \tag{2a}$$

$$\frac{\partial[\text{CaFluo}]}{\partial t} = D_{\text{Fluo}}\nabla^2[\text{CaFluo}] + R_{\text{CaFluo}}, \tag{2b}$$

$$\frac{\partial[\text{CaEGTA}]}{\partial t} = D_{\text{EGTA}}\nabla^2[\text{CaEGTA}] + R_{\text{CaEGTA}}, \tag{2c}$$

$$\frac{\partial[\text{CaS}]}{\partial t} = R_{\text{CaS}}, \tag{2d}$$

where $D_{Ca^{2+}}$, D_{Fluo}, and D_{EGTA} are the diffusion coefficients of Ca^{2+}, Fluo, and EGTA, respectively. The reaction terms R_{CaX} derived from the kinetic scheme, Eq. (1), can be written as

$$R_{CaX} = k_{\text{on}}^X[Ca^{2+}]([X]_T - [CaX]) - k_{\text{off}}^X[CaX]. \tag{3}$$

The Ca^{2+} entry through (open) IP_3R's is included in the boundary conditions [21]. Namely, we consider the cytosolic space as a parallelepiped of sides L_x, L_y, and L_z. The plane $z=0$ represents the surface of the ER membrane, where there are N_s sources of (small) area δS centered at positions $\mathbf{r}_s(i) = (x_s^i, y_s^i, 0), i=1,\ldots,N_s$ [see Figs. 1(a) and 1(b)]. We assume no flux boundary conditions everywhere for all concentrations except for free Ca^{2+} at the location of the sources, where we consider the condition [21]

$$-D_{Ca^{2+}}\frac{\partial}{\partial z}[Ca^{2+}][\mathbf{r}_s(i),t] = J_{\text{ch}} \quad \text{for } i=1,\ldots,N_s, \tag{4}$$

where J_{ch} is the Ca^{2+} flux through the sources. Namely, $J_{\text{ch}} = \frac{I_{\text{ch}}}{(2F\delta S)}$, where I_{ch} is the single channel current (which is equal to zero if the channel is closed) and F is Faraday's constant (96, 485 C mol^{-1}). At the surface of the ER there are also Ca^{2+} pumps that take Ca^{2+} ions back into the lumen of the ER, collaborating to restore and keep $[Ca^{2+}]$ at its basal level. Nevertheless, we do not consider Ca^{2+} pumps because they act in a slower time scale.

In this paper, we solve this full model in two types of situations. In one of them, the N_s Ca^{2+} sources correspond to individual IP_3R-Ca^{2+} channels. In the other one, individual channels are not resolved and the sources correspond to either a finite region within the cluster with several channels inside or to the whole cluster. When individual channels are resolved, we either model their behavior using the stochastic De Young and Keizer model [17] with a type of simulation

that resembles the ones by Swillens *et al.* in Ref. [2] or we assume that they remain open for a finite amount of time that is fixed *a priori*. The purpose of the latter is to analyze the quality of certain approximations in different situations. The kinetic model, on the other hand, assumes that the channels can be in a finite set of states, some of which are open and others are closed, with transition probabilities between states that can depend on $[Ca^{2+}]$ (see the Appendix). When the channels are open we consider that they release a fixed current I_{ch}. When individual channels are not resolved, the time course of the released current is computed separately, as explained later.

All numerical simulations of the model are done using a forward Euler method in time and an explicit finite-difference formula in space with a second order expression (first neighbors) for the Laplacian. Different sizes of the integration region and of the spatial grid are used in different cases. For the initial condition, we assume that all concentrations are homogeneously distributed, Ca^{2+} is at basal concentration and all species are in equilibrium among themselves ($R_{CaX}=0$ for all X), so that

$$[Ca^{2+}](\mathbf{r},t=0)=[Ca^{2+}]_{basal}, \tag{5}$$

$$[CaX](\mathbf{r},t=0)=\left(\frac{k_{on}^{X}[Ca^{2+}]_{basal}}{k_{on}^{X}[Ca^{2+}]_{basal}+k_{off}^{X}}\right)[X]_{T}, \tag{6}$$

where X represents S, EGTA, BAPTA, or Fluo. The physical parameter values are listed in Table I. They correspond to values that have been used in other modeling papers on intracellular calcium dynamics [3,38].

TABLE I. Numerical parameters used to solve the (full) reaction-diffusion model that describes the dynamics of intracellular Ca^{2+} (Sec. II) [3,38].

Parameter	Value	Units
Free Calcium:		
$D_{Ca^{2+}}$	200	$\mu m^2/s$
$[Ca^{2+}]_{basal}$	0.1	μM
Calcium indicator (Fluo4-dextran):		
D_{Fluo}	15	$\mu m^2 s$
k_{on}^{Fluo}	150	$\mu M^{-1}s^{-1}$
k_{off}^{Fluo}	300	1/s
$[Fluo]_T$	40	μM
Exogenous buffer (EGTA):		
D_{EGTA}	200	$\mu m^2/s$
k_{on}^{EGTA}	5	$\mu M^{-1}s^{-1}$
k_{off}^{EGTA}	0.75	1/s
$[EGTA]_T$	300	μM
Exogenous buffer (BAPTA):		
D_{BAPTA}	200	$\mu m^2/s$
k_{on}^{BAPTA}	500	$\mu M^{-1}s^{-1}$
k_{off}^{BAPTA}	100	1/s
$[BAPTA]_T$	300	μM
Endogenous stationary buffer:		
k_{on}^{S}	400	$\mu M^{-1}s^{-1}$
k_{off}^{S}	800	1/s
$[S]_T$	300	μM
Calcium current:		
I_{ch}	0.1	pA

III. A SIMPLIFIED MODEL OF Ca^{2+} DYNAMICS WITHIN A CLUSTER OF IP_3R'S

A. Analyzing the Ca^{2+} distribution near one open channel

In order to build a model capable of describing, in a simplified manner, the coupled dynamics of cytosolic Ca^{2+} and of several IP_3R's within a cluster, we first analyze how $[Ca^{2+}]$ behaves in the presence of a very localized source that opens for a fixed time (i.e., we do not model the channel kinetics in this case). To this end, we performed a series of numerical simulations of the model described in Sec. II assuming that there is only one Ca^{2+} channel present ($N_s=1$) located at $\mathbf{r}_s(1)=(0,0,0)$. We consider a cytosolic space of sides $L_x=2.7$ μm, $L_y=2.7$ μm, and $L_z=1.5$ μm, a grid spacing $dx=dy=dz=20$ nm and time step $dt=0.3$ μs. Results obtained with this dt were indistinguishable from those obtained with smaller values of dt. In the simulations, the channel opens at $t=0$ and releases a constant calcium current (I_{ch}) during 10 ms (a typical open duration for an IP_3R) after which the current becomes equal to zero again. A typical time course of the $[Ca^{2+}]$ at different distances from the source and at the surface of the ER $[(x,0,0),x=0,20,40,\ldots,$ nm], is shown in Fig. 2(a). We will analyze separately what happens before and after the channel closes.

We can see that after the channel opens, $[Ca^{2+}]$ at the surface of the ER tends to a stationary solution that depends only on the distance to the source. Without loss of generality, we will consider the distance along the x coordinate. The time scale to achieve such stationary solution depends on x. We show in Fig. 2(b) the spatial distribution of $[Ca^{2+}](x,0,0,t')$ for different times, t', and we see that it tends to a stationary solution, $C_{st}(x)$ asymptotically in time. Our results agree with previous simulations of the temporal and spatial distribution of free Ca^{2+} in the cytosol around an open channel [23]. In addition, theoretical cytosolic $[Ca^{2+}]$ profiles for different times were already reported in Ref. [22], also showing that the steady state near the channel is quickly established. Here we quantify the differences between the actual profile and the steady profile. We have determined that if we replace $[Ca^{2+}](x,0,0,t)$ by $[Ca^{2+}](x,0,0,10\text{ ms})$ (just before the channel closes) the error inside the cluster region is lower than 10% after a time $t\simeq 3$ ms for $x\leqslant 60$ nm [see Fig. 2(c)]. Therefore, neglecting the $\sim$3 ms transient, we can approximate

$$[Ca^{2+}](x,0,0,t)\approx C_{st}(x)\equiv[Ca^{2+}](x,0,0,10\text{ ms}),$$

$$0<t\leqslant t_{end},\quad x\leqslant 60\text{ nm}, \tag{7}$$

within the cluster region.

In Eq. (7), t_{end} is the time at which the channel closes (here $t_{end}=10$ ms) and we approximate the stationary solu-

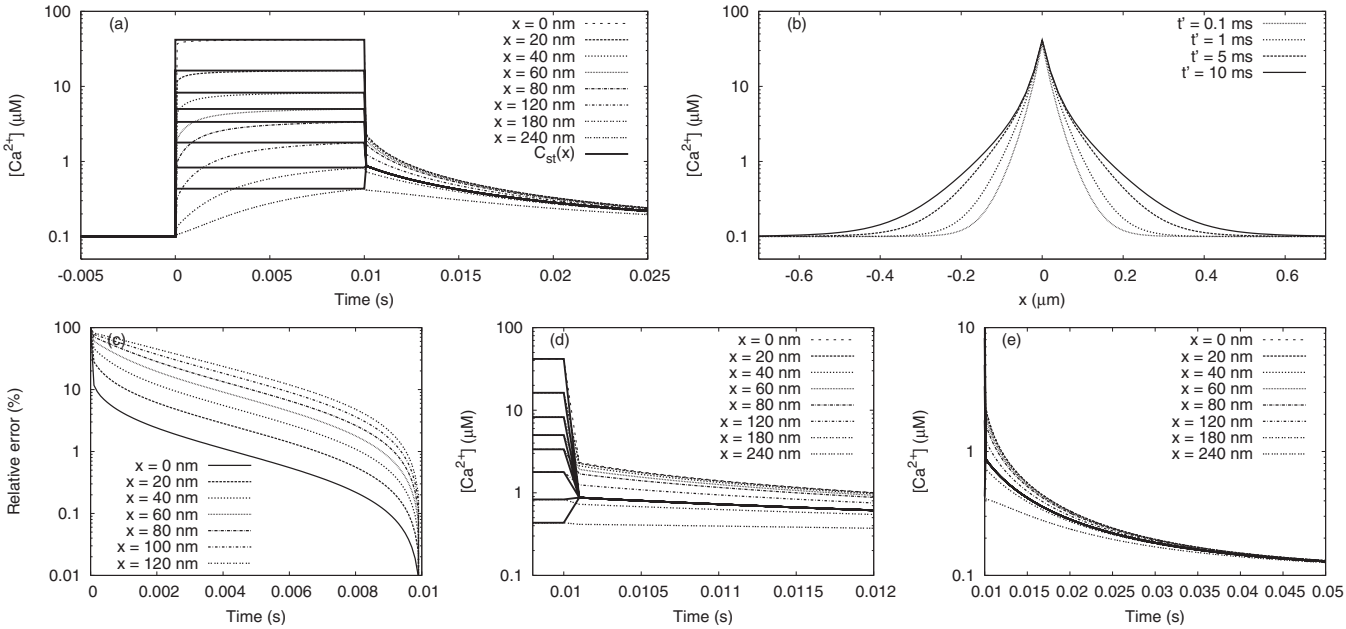

FIG. 2. Results of the simulation of the (full) reaction-diffusion model presented in Sec. II in the presence of one localized source at $\mathbf{r}_s=(0,0,0)$. The source releases Ca^{2+} ions at 0.1 pA between $t=0$ and $t=0.01$ s. (a) Each trace shows $[Ca^{2+}]$ at a different distance x from the mouth of the channel. The solid line for $t<10$ ms represents the $[Ca^{2+}]$ value reached after 10 ms, i.e., $C_{st}(x)$. After the channel closes ($t_{end}=10$ ms), the $[Ca^{2+}]$ decays slowly to its basal level. (b) Spatial profile of $[Ca^{2+}]$ at four times 0.1, 1, 5, and 10 ms (just at the time of the channel closing). (c) Relative difference (in %) between $C_{on}(x)+[Ca^{2+}]_{basal}$ and $[Ca^{2+}](x,0,0,t)$ during the time that the channel is open at different distances from the location of the source $x=0,20,40,\ldots,120$ nm. (d), (e) Results of the simulation of the simplified model (solid lines) and the full reaction diffusion model (dotted lines), after the source located at $\mathbf{r}_s(1)=(0,0,0)$ turns off in regions of the size of a cluster (see Sec. III). According to this model, after the channel closes, $[Ca^{2+}]$ collapses linearly to a common value regardless of the value of x (in a time $t_{collapse}=0.1$ ms) and then it follows a spatially homogeneous decay.

tion in the presence of the open source $C_{st}(x)$ by $[Ca^{2+}](x,0,0,10\ \text{ms})$. The shape of the $[Ca^{2+}]$ distribution depends on the concentrations of buffers in the cytosol. We repeated the simulation described above with other parameters ($[EGTA],[BAPTA]=0,100,200,300\ \mu M$) and we found that the approximation of Eq. (7) holds even better for other concentrations. Indeed, [EGTA] is such a slow buffer (see Table I) that for the concentration values we used, the $[Ca^{2+}]$ does not change significantly. On the other hand, with increasing concentrations of BAPTA the stationary $[Ca^{2+}]$ is achieved in less than 3 ms, due to the fast kinetics of the buffer. Changing the diffusion coefficients of the exogenous buffers does not affect the quality of the approximation either. In particular, we have run simulations using values for these coefficients between 50 and 200 $\mu m^2\ s^{-1}$ and did not observe any appreciable changes in $[Ca^{2+}]$.

We will then use the stationary solution $C_{st}(x)$ to approximate the contribution of each open channel to the $[Ca^{2+}]$ distribution within the cluster region. In order to expedite the subsequent computations, we approximate $C_{st}(x)$ as

$$C_{st}(x) \approx C_{on}(x) + [Ca^{2+}]_{basal} \equiv \sum_{i=1}^{4} A_i e^{-x/\delta_i} + [Ca^{2+}]_{basal}. \tag{8}$$

The fitting function (8) has the purpose of having an analytic expression that approximates $C_{st}(x)$. It depends on the properties of the system that is simulated. However, we have observed that regardless of these other parameters, $C_{st}(x)$ can always be approximated by an expression of the form (8) (at least for [EGTA] and [BAPTA] within the range of 0 $-300\ \mu M$). Equations (7) and (8), on the other hand, imply that $\Sigma A_i+[Ca^{2+}]_{basal}=[Ca^{2+}](0,0,0,10\ \text{ms})$. Other fitting parameter values $\{A_i,\delta_i\}$ are obtained for other values of the single channel current or for other types or amounts of exogenous buffers. The stationary solution near an open channel has been extensively studied in the literature. Using different approximations, researchers have found analytical expressions for the $[Ca^{2+}]$ near an open channel [21,22]. These expressions may be used instead of Eq. (8) if the corresponding approximations used to derive the analytical expressions are valid. Here we choose to use a fitting function that can be used, in principle, beyond the range of validity of the various analytic approximations that can be found in the literature.

We now analyze what happens after the Ca^{2+} channel closes. We show in Figs. 2(d) and 2(e) plots of $[Ca^{2+}](x,t)$ as a function of time for various values of x. It can be observed that soon after the channel closes ($\sim$0.1 ms, a time we call $t_{collapse}$), $[Ca^{2+}]$ becomes almost spatially homogeneous, especially for $x\leqslant 60$ nm [see Fig. 2(d)]. For the purpose of building the simplified model (Sec. III), we will assume that a time $t_{collapse}$ after the channel closes, $[Ca^{2+}]$ becomes homogeneous. The differences in $[Ca^{2+}](x,t=t_{end}+t_{collapse})$ are smaller than 1 μM for $x<60$ nm (the relative error is $\sim$18%). We approximate the fast decay of $[Ca^{2+}]$ between t_{end} and $t_{end}+t_{collapse}$ by a linear function of t. After $t_{collapse}$,

$[Ca^{2+}]$ follows a slower decay leading to its basal level on the order of tens of milliseconds [see Fig. 2(e)]. An analytic expression of this decay can be found by fitting $[Ca^{2+}](x,0,0,t)$ (within the cluster region and for $t > t_{end} + t_{collapse}$) with the following function that depends only on time (in practice we use $x = x^* = 160$ nm):

$$[Ca^{2+}](x,0,0,t) \approx C_{decay}(t) + [Ca^{2+}]_{basal} \equiv \sum_{i=1}^{3} B_i \left(1 + \frac{t - (t_{end} + t_{collapse})}{\tau_i}\right)^{-\alpha_i} + [Ca^{2+}]_{basal}, \quad t > t_{end} + t_{collapse}. \tag{9}$$

We show in Fig. 2(e) $C_{decay} + [Ca^{2+}]_{basal}$ and $[Ca^{2+}](x,0,0,t)$, for different values of x, as functions of time. We can observe the quality of the fit. Again, the purpose of the function C_{decay} is to have an analytic expression of $[Ca^{2+}]$ during the decay so as to make all subsequent computations much faster, as it will be clear in Sec. III. The coefficients B_i must satisfy $\Sigma_{i=1}^{3} B_i + [Ca^{2+}]_{basal} = [Ca^{2+}](x^*, t_{end} + t_{collapse})$. A similar fitting function but with other parameter values can be used in the presence of other types or amounts of buffers and for other values of the single channel current. The goodness of the fit is almost perfect for $x^* = 160$ nm. For other values of $x < 160$ nm, the relative error is a rapidly decreasing function, being lower than 25% for $t - t_{collapse} > 5$ ms.

B. Determining the $[Ca^{2+}]$ distribution within a cluster of IP_3R's

Experimental observations of local Ca^{2+} events in *Xenopus laevis* oocyte indicate that IP_3R's are organized in clusters [5] composed of a few tens of channels within a region of only a few hundreds of nm [2–4]. In this section we use the approximate solutions described in Sec. III A to build a simplified model of Ca^{2+} dynamics within a cluster of IP_3 receptors. We emphasize that given the large gradients of cytosolic $[Ca^{2+}]$ that build up close to an open channel, we will not consider that all the channels in the cluster sense the same $[Ca^{2+}]$.

We consider that the cluster is composed of N_s channels distributed around $\mathbf{r} = \mathbf{0}$ at specified locations $\mathbf{r}_s(i) = (x_s^i, y_s^i, 0)$, $i = 1, \ldots, N_s$ [see Fig. 1(b)]. The number and the distribution of channels within the cluster are based on experimental observations and previous theoretical results [2–4]. The channels can be open or closed, and while they are open they release a constant current I_{ch} (Table I). The model has two main hypothesis. One is to assume that $[Ca^{2+}](\mathbf{r},t)$ within the cluster region can be approximated by a sum of the contributions of the individual channels, so that

$$[Ca^{2+}](\mathbf{r},t) \approx \sum_{i=1}^{N_s} C(R_i,t) + [Ca^{2+}]_{basal}, \quad \text{for } r \text{ within the cluster region} \tag{10}$$

where $R_i = |\mathbf{r} - \mathbf{r}_s(i)|$ and $C(R_i,t)$ is the contribution to $[Ca^{2+}]$, at $\mathbf{r}$, of the ith channel located at $\mathbf{r}_s(i)$. The second hypothesis is that $C(R_i,t)$ can be approximated by a function that only depends on the state of the channel located at $\mathbf{r}_s(i)$. We distinguish four different conditions: the channel has never opened (i), the channel is open (ii), a time less than $t_{collapse}$ has passed since the channel has last closed (iii) or a time larger than $t_{collapse}$ has passed since the channel has last closed (iv). Given the results of Sec. III A, we define $C(R_i,t)$ as follows:

$$C(R_i,t) = \begin{cases} 0 & \text{if the channel has never opened (i)}, \\ C_{on}(R_i) & \text{if the channel is open (ii)}, \\ C_{on}(R_i) + \dfrac{C_{collapse} - C_{st}(R_i)}{t_{collapse}}(t - t_{end}) & \text{if } t_{end} < t \leq t_{end} + t_{collapse}, \text{ (iii)}, \\ C_{decay}(t) & \text{if } t > t_{end} + t_{collapse}. \text{ (iv)}. \end{cases} \tag{11}$$

Also in this case, we either simulate the channel transitions among states using the De Young and Keizer kinetic model [17] or we fix the opening and closing times *a priori*. The purpose of the latter is to analyze the quality of the approximations.

We now compare the distribution of free Ca^{2+} concentration that we obtain with the method just described and the one we obtain by solving the full reaction-diffusion model, with exactly the same conditions, i.e., the same number and location of the channels within the cluster, buffer parameters, etc. All parameters are as described in Table I, using $[EGTA] = 300\ \mu M$ as the exogenous buffer other than the dye. We explain later how we compare both models when the channel kinetics is included in the simulation.

For simplicity, we first consider a cluster of three channels ($N_s = 3$) located at $\mathbf{r}_s(1) = (-120,0,0)$, $\mathbf{r}_s(2) = (0,0,0)$, $\mathbf{r}_s(3) = (120,0,0)$. Channels 1 and 2 open from $t = 0$ s to $t = 0.01$ s while channel 3 opens at $t = 0.005$ s and remains open for 10 ms. We show in Fig. 3(a) the time evolution of $[Ca^{2+}]$ at $\mathbf{r} = \mathbf{0}$ and in the inset we show the spatial distribu-

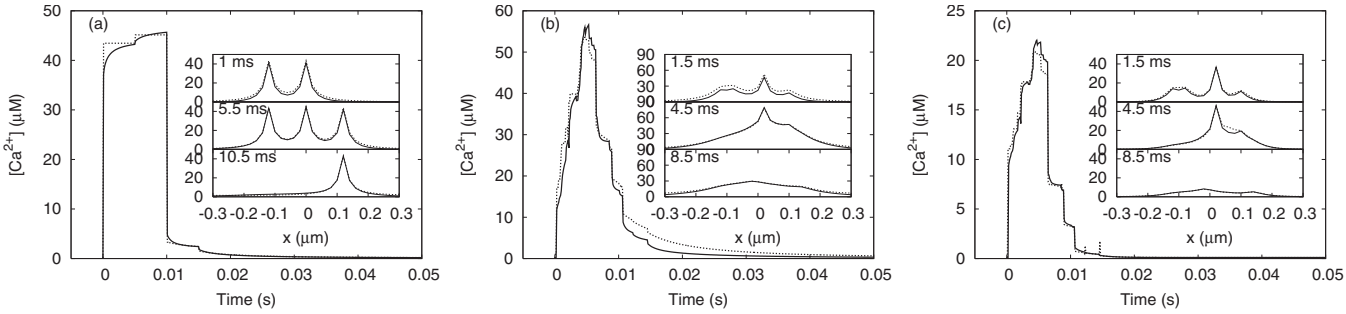

FIG. 3. (a): $N_s=3$ channels are located at the membrane of the ER at points $\mathbf{r}_s(1)=[(-120\ \text{nm},0,0),\mathbf{r}_s(2)=(0,0,0)$, and $\mathbf{r}_s(3)=(120\ \text{nm},0,0)]$. The channels remain open during 10 ms (channels 1 and 2 open at $t=0$ and channel 3 at $t=0.005$ s). We show $[Ca^{2+}](0,0,0,t)$ calculated with the full reaction diffusion model (solid line) and with the SM (dotted line) and in the insets the spatial distributions of free $[Ca^{2+}]$ along a line $(x,0,0)$ at times, 1, 5.5, and 10.5 ms, respectively. (b) Same as (a) but for a cluster of $N_s=20$ channels, located at positions described in Fig. 1(b) and with open and closed times as in Fig. 1(c). (c) Same as (b) but for a cytosol with BAPTA at 300 μM instead of EGTA. In all cases, solid lines plots correspond to results with the full reaction diffusion model and dotted lines with the simplified model.

tion of $[Ca^{2+}]$ along a line at the surface of the ER, for three different times. In all cases we show the results obtained solving the full reaction-diffusion model (solid line) and the simplified model (dotted line). At $\mathbf{r}=\mathbf{0}$ the relative differences were most of the time smaller than 10%. except for brief periods (shorter than 1 ms when a channel opens or closes).

We then consider $N_s=20$ channels in a cluster of 300 $\times$300 nm around $\mathbf{r}=\mathbf{0}$ as in Fig. 1(b). The spatial distribution and the opening and closing times of each channel is chosen arbitrarily and are fixed before starting the simulation. The location of the channels and the time they open and close are summarized in Figs. 1(b) and 1(c). With these parameters we solve the simplified and the full reaction-diffusion models. We show in Fig. 3(b) the time evolution of $[Ca^{2+}]$ at (0,0,0) and in the inset the spatial distribution of $[Ca^{2+}]$ along a line at the surface of the ER, at three different times. Again, we simulated a cytosol with another buffer in order to test the approximation. In Fig. 3(c) we show the results of $[Ca^{2+}]$ simulated in a cytosol with BAPTA at a total concentration of 300 μM. We see that the simplified model gives a $[Ca^{2+}]$ very similar to the solution of the full reaction diffusion model. The absolute error of the simplified model is lower than 5 μM for a cytosol with EGTA and lower than 2 μM for a cytosol with BAPTA. During the period of Ca^{2+} release, the relative errors are most of the time lower than 30% in the case of a cytosol with EGTA and $N_s=20$ channels, and much lower in the cytosol with the faster buffer (BAPTA). After the first 10 ms the relative errors increases because the decay in $[Ca^{2+}]$ is much faster in the full reaction diffusion model than in the simplified model (especially with EGTA). This is not a big problem since it happens after the puff ends, when almost all the channels are closed and it is highly unlikely that they will reopen again due to a low increase in $[Ca^{2+}]$.

Regarding the time it takes for the simulation to be completed, for the cluster of $N_s=20$ channels the full reaction-diffusion model took $\approx$13 min to simulate 1 ms of model time, running on an Intel Xeon 2.66 GHz processor. On the other hand, the time employed by the simplified model was 0.5 s for each ms of model time, in addition to the time needed to run the full model for one open source and find good fitting functions $C_{\text{decay}}(t)$ and $C_{\text{on}}(x)$ as explained in Sec. III A (which is done just one time for each set of conditions of the system and takes $\approx$10 min to simulate 1 ms of model time.

The error of the simplified model cannot be quantified simply by calculating the difference between the $[Ca^{2+}]$ calculated with it and with the full reaction-diffusion model. The behavior of IP_3R's is highly nonlinear. A small difference in $[Ca^{2+}]$ may produce large differences in the behavior of the IP_3R's in the cluster, while for other conditions the channel could be insensitive to changes in $[Ca^{2+}]$. Since we are interested in the behavior of the IP_3R's in the cluster we have to determine whether or not the difference in $[Ca^{2+}]$ affects the stochastic behavior of single IP_3R's.

In order to study to what extent the simplified model is able to reproduce the statistics of the openings and closings of the individual channels of the cluster we solved the simplified and full models in different situations. First, we simulate a case with two channels, one that was located at $\mathbf{r}=0$ which released a constant Ca^{2+} current of 0.1 pA for 10 ms and the other one (test channel), located at a distance x from the first one, that was initially closed and which followed the De Young and Keizer kinetics [17]. The initial state of the closed channel was chosen randomly according to its stationary probability with $[Ca^{2+}]=[Ca^{2+}]_{\text{basal}}$ and $[IP_3]=10$ μM. By doing so, we are assuming that $[IP_3]$ has been constant for a long time so that the channel can be assume to be in a state given by the stationary distribution with the constant $[IP_3]$. Results showing the temporal and spatial distribution of $[Ca^{2+}]$ using the full reaction diffusion and the simplified models are shown in Fig. 2. We show in Fig. 4(a) the mean time for the second channel to open for the first time (latency) as a function of the distance to the open channel, x. The stochastic transitions were computed using the value of $[Ca^{2+}]$ at the mouth of the test channel. We can see that the difference between the expected latency period using the $[Ca^{2+}]$ calculated with the full reaction diffusion and simplified models is negligible [even though the differences in $[Ca^{2+}]$ were not, for example for example for distances from the source as large as 0.5 μm, as shown in Fig. 2(a)]. On the

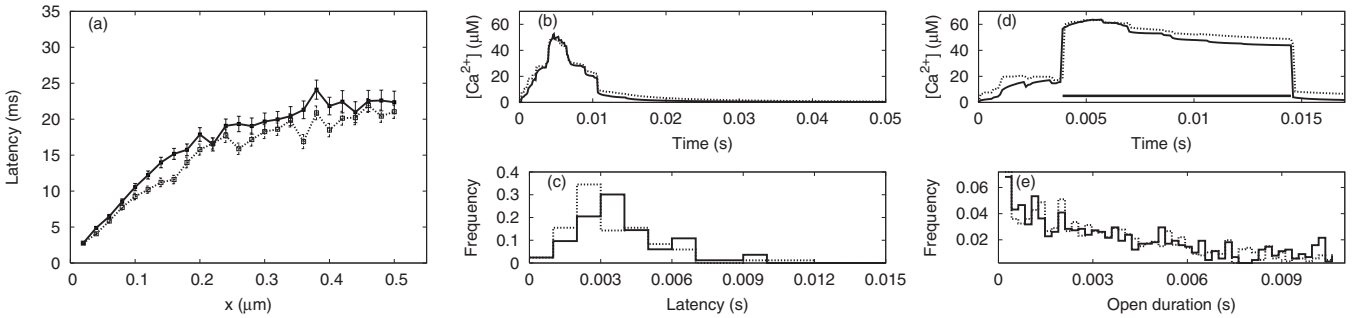

FIG. 4. Different results of IP_3R responses in the presence of different $[Ca^{2+}]$ distributions calculated using the full reaction diffusion and the simplified models. (a) A closed IP_3R (test channel) is located at a distance x from an open channel that releases Ca^{2+} at a constant rate during 10 ms. The IP_3R follows the DeYoung-Keizer stochastic kinetics, so its dynamics is regulated by the local $[Ca^{2+}]$. We measure the latency of the receptor (time to open) when $[Ca^{2+}]$ is obtained by a numerical solution of the full reaction diffusion model and when $[Ca^{2+}]$ is calculated with the simplified model. For each distance x we did 1000 stochastic simulations. We plot the average latency of all these simulations. The error bars are $\frac{SD}{\sqrt{N}}$, where SD is the standard deviation of the latency and N the number of latencies considered (solid lines represents latency obtained with $[Ca^{2+}]$ from the full reaction diffusion model and dotted lines with $[Ca^{2+}]$ from the simplified model). (b) $[Ca^{2+}]$ at $(40,-40,0)$ nm calculated using the full reaction diffusion and the simplified models for the cluster of $N_s=20$ channels. (c) Latency distribution of the test channel (initially closed) located at $(40,-40,0)$ nm.(d), (e) In this case an open IP_3R that follows DeYoung-Keizer stochastic model is located at the location of an open channel within the cluster of $N_s=20$ channels. Horizontal solid line in (d) represents the time during which the channels remains open in the simulation of the full reaction diffusion and the simplified models (the stochastic IP_3R cannot have an open channel longer than that). Solid lines correspond to simulation with $[Ca^{2+}]$ obtained with the full reaction diffusion model and dotted line with the simplified model.

other hand, the latency increases with the distance between both channels (x) which follows immediately from the fact that $[Ca^{2+}]$ tends to $[Ca^{2+}]_{basal}$ for large x [see also Fig. 2(a)].

The computation described previously describes a situation in which there is only one open channel, for instance, when the puff is starting. We then repeated the same type of computation but in the presence of $N_s=20$ IP_3R's in the cluster. We considered a region of 700 nm wide around the cluster and a grid of 20 nm in it. Therefore a total of 35^2 locations are defined, 20 of which are occupied by channels of the cluster. We placed the test channel (initially closed) at a free point of the grid (where there was not already another channel). Then we computed the stochastic transitions of the test IP_3R using again the De Young-Keizer model [17], until the channel opens (latency), in the presence of the time dependent $[Ca^{2+}]$. We computed 200 stochastic latencies using this procedure (100 with $[Ca^{2+}]$ from the full reaction diffusion and 100 with the simplified model). In Fig. 4(b) we show the time evolution of $[Ca^{2+}]$ at the position of the test channel, $(40,-40,0)$ nm. In Fig. 4(c) we show the histograms of latencies of the two sets of data, using simplified or the full reaction diffusion models for $[Ca^{2+}]$. We see that the two sets of latencies are consistent. We repeated this procedure locating the test channel in every free point of the grid and we found that the sets of latencies are consistent in more than 70–80 % of the cases.

Finally, we looked at the $[Ca^{2+}]$ distribution at a point where there was already an open channel and measure the open duration of a test channel located at that point in space and being exposed to the Ca^{2+} obtained with the simplified and full reaction diffusion models. We use, again, the De Young-Keizer model for the channel kinetics. We took the channel that remains open for the longest time [see Fig. 1(c)]. In Fig. 4(d) we show the time evolution of $[Ca^{2+}]$ in both cases and in Fig. 4(e) the open time distribution (limited to the obvious constraint of being lower than the actual open duration of channel 2). Again we see that the two sets of data are consistent.

IV. THE Ca^{2+} AND CaFluo SPATIOTEMPORAL DISTRIBUTIONS OUTSIDE THE CLUSTER REGION

We have shown that the simplified model reproduces the $[Ca^{2+}]$ distribution inside the cluster region with a maximum error of 5 μM for a cytosol with EGTA and 2 μM for a cytosol with BAPTA. The relative error stays below 20% for a cluster of 20 open channels (but is much slower for a smaller cluster). Furthermore, the errors are small enough so that the statistics of the openings and closings of the channels in the cluster are reproduced correctly. In spite of this, the results are not readily comparable to the experimental observations, even for isolated events such as puffs. Namely, optical experiments give information on the Ca^{2+}-bound to dye distribution averaged over a region of size $\sim$300 nm $\times$300 nm$\times$700 nm, which is larger than the one spanned by a typical cluster. The simplified model described before is not good enough to describe the $[Ca^{2+}]$ distribution within this larger region. Furthermore, if one is willing to model global Ca^{2+} signals that propagate throughout the cell, it is necessary to describe the spatiotemporal distributions of $[Ca^{2+}]$ and Ca^{2+} bound to dye over much larger regions (involving $\sim$ mm distances). To this end, we simulate the full reaction-diffusion model.

To obtain the distribution of $[Ca^{2+}]$ and [CaFluo] outside the cluster region we solve the full reaction-diffusion system described in Sec. II but using a "coarse" spatial grid (that can be larger than a typical cluster size). In this section we analyze how coarse the grid may be and still give the $[Ca^{2+}]$ and [CaFluo] distributions with relatively low errors. We also analyze to what extent the clusters can be replaced by point

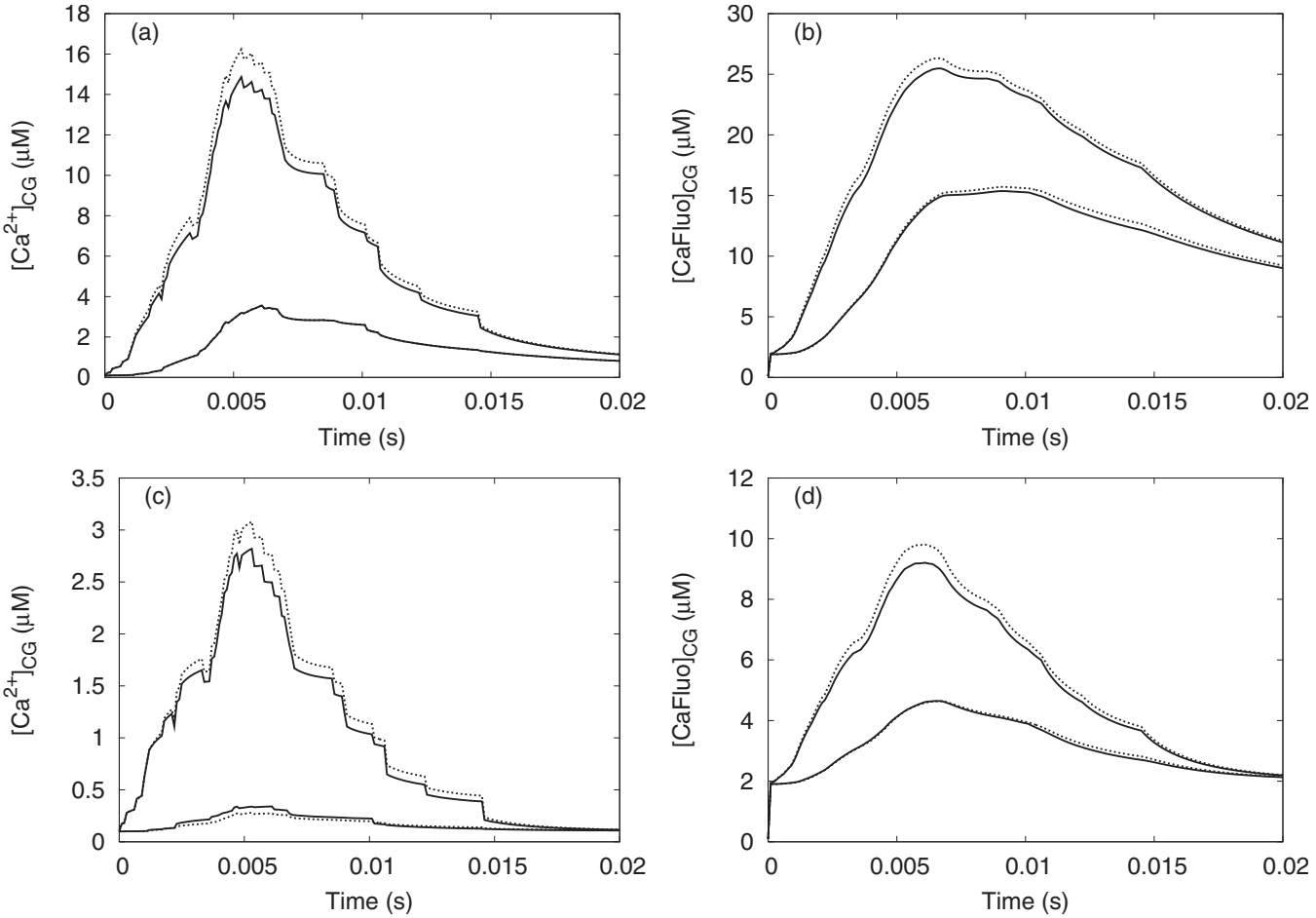

FIG. 5. Comparison of the time evolution of $[Ca^{2+}]$ and [CaFluo] coarse grained over a region of $(300\ \text{nm})^3$ around $\mathbf{r}_1=0$ and around $\mathbf{r}_2=(300,0,0)$ using two discretizations to solve the full reaction diffusion model [$dx=dy=dz=20$ nm (solid lines) and $dx=dy=dz=100$ nm (dotted lines)]. (a), (b) with EGTA at a total concentration of 300 μM and (c), (d) with BAPTA also at 300 μM of total concentration. In each plot, the two curves with higher concentration values correspond to $\mathbf{r}_1$ and the lower ones to $\mathbf{r}_2$

sources for which the total Ca^{2+} current is the one determined using the simplified cluster model, regardless of the number of channels that are open at any given time. To test the accuracy of the approximation, we compare the solutions obtained using the full reaction diffusion model with different discretizations: some in which each channel of the cluster is contained in a different grid point and others in which several channels of the cluster belong to the same grid point. In the latter, the Ca^{2+} current is simply calculated as the sum of the currents that flow through each open channel at any given time, i.e., in Eq. (4), $J_{\text{ch}}=\frac{1}{(2F\delta S)}\Sigma I_{\text{ch}}(i)$, where the sum is over all channels that are located at the same grid point and $\delta S=dxdy$, with dx and dy the grid spacing. In order to perform the comparison, we coarse grain all the solutions so as to represent them with a spatial resolution that is similar to the experimental one [$\sim(300\ \text{nm})^3$]. Namely, we compute

$$[Ca^{2+}]_{CG}(\mathbf{r}=\mathbf{0},t)=\int_{\Delta V}[Ca^{2+}](\mathbf{r},t)dV, \qquad (12)$$

$$[\text{CaFluo}]_{CG}(\mathbf{r}=\mathbf{0},t)=\int_{\Delta V}[\text{CaFluo}](\mathbf{r},t)dV, \qquad (13)$$

where ΔV is a volume of $(300\ \text{nm})^3$ defined as $-\Delta x/2\leqslant x\leqslant\Delta x/2$, $-\Delta y/2\leqslant y\leqslant\Delta y/2$, and $0\leqslant z\leqslant\Delta z$ ($\Delta x=\Delta y=\Delta z=300$ nm).

We show in Fig. 5 the time evolution of $[Ca^{2+}]_{CG}$ and $[\text{CaFluo}]_{CG}$ at $\mathbf{r}_1=(0,0,0)$ and at $\mathbf{r}_2=(300\ \text{nm},0,0)$ obtained for the case with $N_s=20$ channels already described in Sec. III and Figs. 1(b) and 1(c). Figures 5(a) and 5(b) are simulations with EGTA and Figs. 5(c) and 5(d) with BAPTA. The two solutions displayed correspond to grid sizes: $dx=dy=dz=20$ nm (solid lines) and $dx=dy=dz=100$ nm (dotted lines). In each plot, the couple of curves with higher concentration values correspond to $\mathbf{r}_1$ while the other two correspond to $\mathbf{r}_2$. The differences are a little larger in $\mathbf{r}_1$ than in $\mathbf{r}_2$ but in all cases the absolute differences are not significant in μM. The relative differences in $[\text{CaFluo}]_{CG}(\mathbf{r}=\mathbf{0},t)$ is always below 6% (at $\mathbf{r}_1$ and $\mathbf{r}_2$, either with EGTA or BAPTA). In the case of $[Ca^{2+}]_{CG}(\mathbf{r},t)$ the relative differences are below 10% in the case of a cytosol with EGTA and in the case of

BAPTA it is a little larger because the absolute difference is similar but the total $[Ca^{2+}]$ is lower since it is mostly bound to the fast buffer, BAPTA.

V. PUFF SIMULATIONS: PUTTING EVERYTHING TOGETHER

The various approximations described so far can be combined to generate the simulation of an isolated Ca^{2+} puff. The steps involved are as follows

(1) Define the components of the cytosol (concentrations and reaction rates) and the single channel Ca^{2+} current (here given in Table I). This last condition can be relaxed and various Ca^{2+} currents can be considered. In such a case, the second step of this list has to be repeated to analyze the behavior of cytosolic $[Ca^{2+}]$ for the various Ca^{2+} currents of interest. The case in which the evolution of cytosolic Ca^{2+} needs to be coupled to the evolution of $[Ca^{2+}]$ inside the ER could be treated similarly. However, the variety of possible Ca^{2+} currents makes the suggested model not very practical in this case.

(2) Solve Eqs. (2) with one point source at $\mathbf{r}=0$ that opens at $t=0$ and remains open for a long time, t_{end} ($t_{end}=10$ ms seemed to be enough in the cases we tried) and then becomes closed again. While the source is on, the cytosolic $[Ca^{2+}]$ in the vicinity of the open channel approximately reaches a stationary solution.

(3) Find (for each current of interest) a good fit of the stationary spatial distribution of $[Ca^{2+}]$, $C_{st}(x) \equiv [Ca^{2+}](x,0,0,t_{end})$ while the channel is open and of its decay after the channel closes, for example using a linear function for a fast decay and a spatial independent function [like $C_{decay}(t)+[Ca^{2+}]_{basal}$], for subsequent times.

(4) Define the number N_s and location $\mathbf{r}_s$ of the channels in the cluster and choose a kinetic model to describe their states and state transitions.

(5) Start your simulation with all channels in a closed state and Ca^{2+} and other components in equilibrium, with $[Ca^{2+}]$ at its basal level. Run the kinetic model for the channels of the cluster under these conditions. As soon as one channel opens, compute $[Ca^{2+}]$ within the cluster using Eqs. (10) and (11). Continue the simulation until all channels are closed again.

(6) The previous step provides information on the time evolution of the total Ca^{2+} current released at the cluster of interest. Solve Eqs. (2) using this current and a coarse spatial grid so that the cluster is fully contained within one grid point. If the time course of the current is known with a finer temporal resolution than the time step with which the full reaction-diffusion model is updated, then, the current needs to be coarse grained in time. If necessary, the Ca^{2+}-bound to dye distribution obtained with the simulation [CaFluo], can be coarse-grained even further to compare with experiments.

Steps 2 and 3 may be avoided if one has an accurate theoretical analytic expression for the stationary $[Ca^{2+}]$ profile close to an open channel such as the ones reported in Refs. [21,22] and for the temporal decay of $[Ca^{2+}]$ after the channel closes. Regarding the time it takes to obtain the fluorescence signal and $[Ca^{2+}]$ during a puff event, our simulations showed that the simple model takes ~25 ms for each ms of model time, which represents a simulation ~60 times faster than the full reaction diffusion model.

VI. GLOBAL Ca^{2+} SIGNALS

Now, the aim of the model is not just to reproduce the dynamics of isolated signals. We also want to use it to describe global Ca^{2+} signals such as waves that propagate throughout the cell as have been observed in various cell types [14,39–44]. These waves can travel in two modes: with no deformation (continuous propagation) or in a saltatory manner (as a sequence of bursts). For instance, in immature *Xenopus* oocytes the propagation is saltatory while the fertilization wave in the mature oocyte is continuous. The "fire-diffuse-fire" model [24] mentioned in Sec. I was able to explain the transition between these two modes of propagation without having a detailed description of the intracluster dynamics. The model introduced in this paper can be used to study this problem from a different perspective in which a more detailed description of the cluster dynamics is included. Recently, it has been shown that for different cell types, global Ca^{2+} oscillations are stochastic, i.e., the result of random occurring Ca^{2+} spikes [45]. Furthermore, the analysis shows that waves initiate randomly (not as the result of a deterministic process) [45]. Our approach of modeling Ca^{2+} waves using a stochastic model for the IP_3R as the elementary unit is particularly suited to study this type of processes. In this section we show how the model can be generalized to simulate the dynamics of intracellular Ca^{2+} in the presence of several clusters of IP_3R's. We also present some simulations that reproduce the propagation of saltatory waves with a velocity that is in agreement with experimental results in *Xenopus laevis* oocytes [14,42].

In the case of considering several clusters we can proceed in the following way. We first choose the location and size of the clusters and the distribution of IP_3R's inside each of them. Let us call dx, dy, dz the grid spacings within the cluster region and Δx, Δy, and Δz the grid spacings outside. Let us consider square clusters of sides of size $\Delta x = Ndx$ and $\Delta y = Ndy$. Only one channel is contained in a $dx \times dy$ region, while the whole cluster is contained inside the $\Delta x \times \Delta y$ region. Again we start from a situation in which all channels are closed and Ca^{2+} is uniformly distributed and in equilibrium with all other species at its basal level. Depending on the situation that we want to model, we can either run the kinetic IP_3R model, use probability arguments to decide when the first channel opens or we can put one randomly chosen channel in an open state at $t=0$. Once the first channel opens we compute separately the $[Ca^{2+}]$ distribution within the clusters (using the dx, dy, dz grid spacings) and in the region outside (which is resolved up to Δx, Δy, and Δz). Let us assume that the channel kinetics within the cluster is followed with a time step dt and that the reaction-diffusion model outside the cluster regions is updated with a larger time step Δt. For simplicity, we take $\nu \equiv \Delta t/dt$ to be integer. Let us call $[Ca^{2+}]_{LR}$ the Ca^{2+} concentration computed with the large grid spacing and large time step (Δx, Δy, Δz and Δt, respectively) and $[Ca^{2+}]_{HR}$, the high resolution (dx, dy,

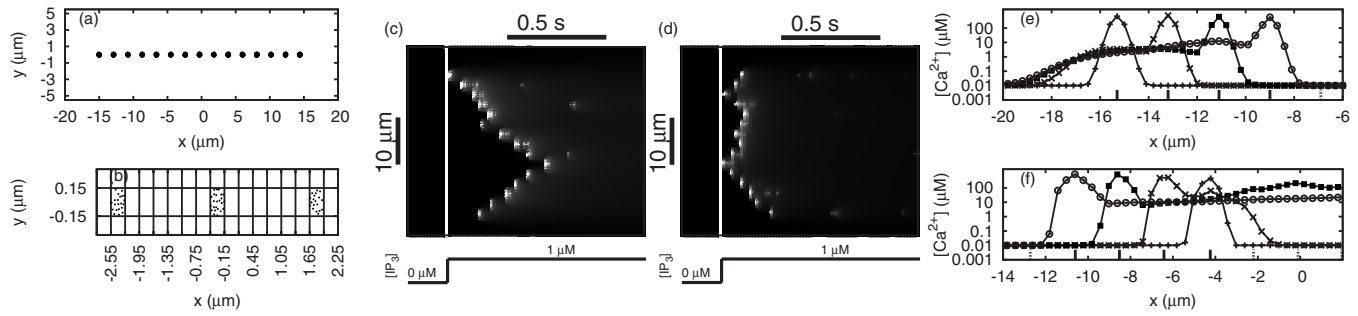

FIG. 6. Results of the simulation of global Ca^{2+} signals in the presence of several cluster of channels. (a) A sketch of the cytosolic space where we simulate Ca^{2+} dynamics. Note that all clusters are located at the line $(x,0)$ and separated by 1.2 μm. (b) A more detailed look at the channels and clusters distribution. It is also showed the grid we use for the low spatial resolution step of simulations ($\Delta x=300$ μm). (c), (d) Typical space time (linescan) images of $[Ca^{2+}]$ in the plane (t,x). Brighter regions means elevated $[Ca^{2+}]$. Time advances from left to right. (c) corresponds to the simplified model and (d) to the full reaction diffusion mode. White vertical line correspond to the time of IP_3 release. We can see several traveling waves (e), (f): Four snapshots of the spatial distribution of $[Ca^{2+}]$ showing a saltatory wave, at four different times: (e) Simplified model: $t=322$ ms (+), $t=428$ ms (×), $t=527$ ms (black square) and $t=572$ ms (open circle). (f) Full reaction diffusion model: $t=7$ ms (+), $t=48$ ms (×), $t=101$ ms (black square), $t=145$ ms (open circle). Each snapshot corresponds to the time at which one cluster is firing. Vertical lines shows the location the clusters (solid if the cluster fired and dashed if the cluster did not fire in any of those four times). Note that at each time there is only one cluster firing.

dz, and dt) concentration computed within one particular cluster. Let us assume that we have already updated $[Ca^{2+}]_{LR}$ at time $t=n\Delta t$ and that we want to move one (large) time step with the simulation. Let us describe how we would proceed with one particular cluster between $n\Delta t$ and $(n+1)\Delta t$ (all clusters should be updated "simultaneously," following the same approach). This implies computing the intracluster dynamics during ν time steps of size dt. To this end, we run the channel kinetic model for each channel of the cluster updating $[Ca^{2+}]_{HR}$ inside the cluster at the same time using Eq. (11) and a modified version of Eq. (10) of the form

$$[Ca^{2+}]_{HR}(\mathbf{r},t) = \sum_{i=1}^{N_s} C(R_i,t) + [Ca^{2+}]_0(n\Delta t)n\Delta t + dt \leqslant t \leqslant n\Delta t + \nu dt, \tag{14}$$

with

$$[Ca^{2+}]_0(n\Delta t) = \begin{cases} [Ca^{2+}]_{LR}(n\Delta t) - \left[\left\langle \sum_{i=1}^{N_s} C(R_i,n\Delta t)\right\rangle\right] & \text{if } [Ca^{2+}]_{LR}(n\Delta t) - \left[\left\langle \sum_{i=1}^{N_s} C(R_i,n\Delta t)\right\rangle\right] \geqslant [Ca^{2+}]_{basal}, \\ [Ca^{2+}]_{basal} & \text{otherwise,} \end{cases} \tag{15}$$

where $\langle\cdots\rangle$ is an average over all grid points inside the cluster. The term $[Ca^{2+}]_0(n\Delta t)$ is the average $[Ca^{2+}]$ within the cluster minus the contribution to this average due to the channels of the cluster itself. $[Ca^{2+}]_0$ is responsible for the possible coupling between clusters. Given that $[Ca^{2+}]_0$ represents the contribution of other clusters to the $[Ca^{2+}]$, we consider its variation only on the low resolution scale. However, as explained later, there was no need to consider $dt<\Delta t$ and, all the results that we show have been obtained for $dt=\Delta t$.

The computation (14) is repeated ν dt time steps. At the end, we compute the total current that flew through each cluster between $n\Delta t$ and $(n+1)\Delta t$ as before, by simply adding the current that flew through each open channel at any given time. We are then in the position of advancing one Δt time step the full reaction-diffusion system Eqs. (2) with $J_{ch}=\frac{1}{(2F\delta S)}\Sigma I_{ch}(i)$, where the sum is over all channels that are located at the same (coarse) grid point and $\delta S=\Delta x\Delta y$. Given that we do not simulate Ca^{2+} diffusion inside the cluster but use some analytic approximation, it is the transition rates among the channel states that determine the allowed values of dt. Thus, we do not need to use $dt<\Delta t$ and in all the simulations that we present we have used $dt=\Delta t$, i.e., $\nu=1$.

We performed several simulations using the procedure stated above. We simulated global Ca^{2+} signals generated by a set of N_c clusters arranged in a 1D "chain" within a two-dimensional cytosolic space. In Fig. 6(a) we show the complete cytosolic space and the clusters. The number of channels of each cluster were chosen randomly from a Poisson distribution with a mean of 25 IP_3R's [4]. The channel locations within the clusters were also picked at random using a uniform distribution over a circle of radius 150 nm. Configurations that gave interchannel distances that were smaller than 40 nm were discarded. We set $\Delta x=\Delta y=300$ nm, so as

TABLE II. Parameters used in the simulation of global Ca^{2+} signals such as the waves shown in Fig. 6. The rest of the parameters are the same as Table I.

Parameter	value	Parameter	value
$dx=dy=dz$	15 nm	N_c	26
$\Delta x=\Delta y$	300 nm	d	1.2 μm
$dt=\Delta t$	5 μs	N_s	Poisson (25)
$[Ca]_{basal}$	0.01 μM	$[EGTA]_T$	0
$[IP3]_{stim}$	1 μM		

to ensure that each cluster corresponded to a single grid point and the intercluster distance is 1.2 μm [see Fig. 6(b) for a closer look at the clusters and channel distribution where the grid lines correspond to the lattice that we used to solve the model in low resolution]. To calculate $[Ca^{2+}]_{HR}$ we used $dx=dy=\frac{\Delta x}{20}=15$ nm. The simulations were done with $[EGTA]=0$. The initial condition was such that $[IP_3]=0$. The channels were modeled using DeYoung-Keizer model [17] and their initial state was chosen randomly using the stationary probability distribution with $[Ca^{2+}]=[Ca]_{basal}$ and $[IP_3]=0$ (see the Appendix for more details). $[IP_3]$ was stepped uniformly in space from 0 μM to $[IP_3]_{stim}=1$ μM at the time indicated by the white horizontal line. The parameters used in these simulations are summarized in Table II.

We first did a simulation with $[Ca^{2+}]_{basal}=0.1$ μM and found that very soon after the IP_3 was released all the channels opened (in a time much shorter than the intercluster diffusion time). In fact, the latency of the IP_3R's is very short after such a step in $[IP_3]$ for the De Young and Keizer model. Therefore, we decreased $[Ca^{2+}]_{basal}$ in order to enlarge the latency and allow intercluster "communication" due to Ca^{2+} diffusion.

In Figs. 6(c) and 6(d), we show linescan images of $[Ca^{2+}]$. The vertical axis represents the position along the line $y=0$, -20 $\mu m \leqslant x \leqslant 20$ μm and the horizontal axis represents time. We can see that several saltatory waves are elicited. The velocity of the waves are between 26 and 42 $\frac{\mu m}{s}$. Figure 6(c) corresponds to the simplified model and Fig. 6(d) is a solution using the full reaction diffusion model. We can see that the results are quite similar. Indeed, in these case the resulting velocities are between 40 and 49 $\frac{\mu m}{s}$. The velocity of the waves obtained in simulations are in the range of saltatory wave velocities found in experimental results in *Xenopus* laevis [14,42].

In Figs. 6(e) and 6(f) we show four snapshots of the spatial distribution of $[Ca^{2+}]$ along a segment of the line $(x,0)$ at different times, corresponding to the moments at which four adjacent clusters fire (at the peak of its Ca^{2+} release). The short vertical lines at the horizontal axis indicate the position of the clusters (solid lines are clusters with open channels at one of the times shown and dotted lines are clusters that are closed at the four times shown). Note that only one cluster "fires" (releases Ca^{2+}) at a time (saltatory propagation) and that after the cluster fired, $[Ca^{2+}]$ at its location decreases back to its basal value. Figure 6(e) correspond to the simplified model (wave traveling from left to right) and Fig. 6(f) to the full reaction diffusion model (wave traveling from right to left).

Again, the improvement in computer time using the simplified model was considerable. The simplified model takes $\sim 15s$ per ms of model time while the full reaction diffusion model takes ~ 6 min to simulate the same model time (all values measures in simulations running on a Intel Xeon 2.66 GHz processor).

VII. CONCLUSIONS

The development of microscopy and fluorescent indicators have made it possible to measure localized Ca^{2+} signals that result from the activity of clustered channels in the membrane of the endoplasmic reticulum. On one hand, these optical techniques have the advantage over electrophysiological single channel recordings that they are less invasive and provide spatial information. On the other hand, due to their spatial and temporal resolution, they are still unable to resolve in detail the activity of channels within a cluster or to allow the study of the kinetics of single IP_3R's as in patch-clamp recordings. Therefore, the use of mathematical models is a useful tool to gain insight and to understand local and global Ca^{2+} signals such as puffs and waves in terms of the activity of their individual units (i.e., the IP_3R-channels).

One of the main difficulties of modeling Ca^{2+} dynamics with discrete source terms resides on the large range of temporal and spatial scales that are involved. Stochastic single channel transitions occur on time scales of ms while the concerting activity of channels produce Ca^{2+} signals that may last for seconds. At the same time, Ca^{2+} release from individual channels produce steep concentration gradients in the vicinity of the open channels (over a ~ 100 nm scale) while the summation of these releases can give rise to Ca^{2+} waves that travel throughout the entire cell ($1-2\sim$ mm in the case of the *Xenopus laevis* oocytes). In this work we introduce a model of cytosolic Ca^{2+} dynamics in the presence of one or several clusters of Ca^{2+}-release channels, each of which is composed of discrete Ca^{2+} sources that behave stochastically. The model is able to span several orders of magnitude in space and time, ranging from the single IP_3R activity to the generation of Ca^{2+} waves. We have tested the model by performing extensive numerical simulations that show its accuracy compared to standard methods. Therefore, we think it gives a good framework to advance in the direction of understanding the local and global dynamics of Ca^{2+} signals in a comprehensive way.

A key aspect of our model is its ability to link efficiently a relatively detailed spatial and temporal description of the stochastic behavior of several IP_3R's in a cluster to the dynamics on a coarser scale in time and space. Previous works on modeling Ca^{2+} dynamics have used other strategies to deal with the problem of the different time and spatial scales involved. In general, this alternative strategies either simplify the diffusion description or the kinetics of single Ca^{2+} channels. A first simple approach is to focus on the temporal dynamics, i.e., to study temporal oscillations discarding diffusion as done by De Young and Keizer in Ref. [17]. One step further would be to consider cytosolic Ca^{2+} diffusion.

Sneyd *et al.* [46] studied wave propagation in pancreatic and parotid acinal cells which result from Ca^{2+} release from IP_3R and ryanodine receptors (RyR) distributed heterogeneously through the cell. The authors included Ca^{2+} diffusion and described the state of the channels using rate equations derived from mass action kinetics that were coupled to an equation governing the evolution of the Ca^{2+} concentration. The distribution of the various receptors was described in terms of densities that were assumed to be nonhomogeneous to reflect the nonuniform localization of IP_3R's and RyR's in the cell type of interest. Another approach presented in the literature was to model in more detail the stochastic nature of the channels but simplifying the diffusion of Ca^{2+} [31,32]. In those works, the authors assumed that $[Ca^{2+}]$ at one cluster depended only on the number of nearest release sites where there were open channels and that each neighboring (active) site added a time-independent contribution to $[Ca^{2+}]$. One useful simplified approach was to discard all detail within the clusters [24] and describe several aspects of global waves considering the clusters as single excitable units. A much detailed description was introduced by Falcke [47,48] to study intracellular Ca^{2+} dynamics in the presence of several clusters of IP_3R's. Each cluster was composed by a certain number of channels that made stochastic state transitions. It was assumed in these works that the size of the cluster was proportional to the number of open channels and within this region, $[Ca^{2+}]$ gradients were neglected, so that $[Ca^{2+}]$ within the cluster was considered homogeneous. This assumption was also used in other works [25,30] and allowed for faster simulations since then the whole cluster could be considered as a single source. Additionally, in several instances, only one cluster was considered, in which case the system is spherically symmetric. This approximation has shown to be useful to describe several experimental observations. Nevertheless, it becomes inadequate if one is interested in modeling the stochastic behavior of single IP_3R's in the presence of Ca^{2+} feedback. Each channel behavior depends on the local Ca^{2+} concentration which is, as we reported in Sec. III A, subject to high $[Ca^{2+}]$ gradients that develop in the vicinity of an open IP_3R, in agreement with previous works [18,21,23,33,34]. If one is willing to include a more accurate description of the Ca^{2+}-release process kinetics, which depends on the time at which each channel of the cluster becomes open, it is necessary to have a better estimate of the $[Ca^{2+}]$ value at each channel pore within the cluster. IP_3R's open and close depending on the local $[Ca^{2+}]$. Therefore it is important to know $[Ca^{2+}]$ close enough to the channel. The model we present in this paper does not rely on the hypothesis of $[Ca^{2+}]$ homogeneity within the cluster. It simplifies the description of the $[Ca^{2+}]$ otherwise.

More recently, large scale computer simulations have been used to model Ca^{2+} dynamics using finite elements methods [49,50]. This type of approach gives much more detail but is computationally more expensive than ours. In Ref. [49] the authors studied Ca^{2+} waves in ventricular and atrial myocites focusing on the influence of the RyR distribution on these waves. One of the simplifications of the model was to use a steady state response of the channel, which allows one to do faster simulations. On the other hand, in Ref. [50], the authors introduced a reaction-diffusion model of Ca^{2+} dynamics with a realistic ER geometry and where the gating of the IP_3R's was modeled stochastically using a five-state representation. Nevertheless, it was not used so far to study global Ca^{2+} signals such as waves.

Our model is built up upon a detailed analysis of the $[Ca^{2+}]$ profile close to a channel when it is open and after it closes. The profiles due to a single channel has been the subject of several works both analytical [21] and numerical [22,23,35]. Here we decided to solve numerically the complete reaction-diffusion system for a particular cytosolic environment with one channel at the center of the cytosol. Finding good fits of both the stationary distribution and the temporal decay of $[Ca^{2+}]$, the solution inside a cluster of several channels is approximated by a superposition of these single channel solutions. We simulated a cluster of IP_3R's with deterministic open and close times and found that the model correctly describes the free $[Ca^{2+}]$ within the cluster of IP_3R's with an error lower than 30%. Furthermore, we also showed that the errors in $[Ca^{2+}]$ do not affect the statistical properties of the channels behavior. We did it by using a specific single IP_3R model and exposing it to the $[Ca^{2+}]$ calculated using the model. We compared the statistics of the latencies and open times obtained in this way with those obtained using a numerical solution of the complete reaction diffusion system.

The use of steady state solutions for the complete reaction diffusion problem in the presence of a single channel has been used previously [21,34,47]. Nevertheless, as pointed out by Bentele and Falcke [22] this approximation is rather poor if used on the whole cell. Therefore, they propose the use of a quasi-steady state approximation that avoids this problem by using stationary solutions over short length scales close to the open channel. Our work resembles this idea by using a stationary $[Ca^{2+}]$ distribution for each open channel within the scale of the cluster. Nevertheless, in this work we do not use analytical expressions for the $[Ca^{2+}]$ distribution near an open channel [21,22,34] to avoid the limitations of the hypothesis that underlie analytic solutions.

We have shown that the model correctly describes the free Ca^{2+} concentration within a cluster of IP_3R's, something that is necessary to connect the reaction-diffusion of Ca^{2+} with the single channel behavior. The model also provides a good approximation to the $[Ca^{2+}]$ and [CaFluo] distributions in a large cytosolic region. The former is needed to model Ca^{2+} signals such as waves that depend on the "communication" between clusters and the latter allows us to make the link with experimental data. In a comparison with a traditional (full) reaction diffusion scheme, this model solves the problem between 25–100 times faster (depending on the parameters and cytosolic space) at a negligible cost. This model opens the door for future work on modeling localized Ca^{2+} signals such as "puffs" (Ca^{2+} release from one cluster) in order to test hypotheses on IP_3R's. Regarding global Ca^{2+} signals, we have shown that the model reproduces saltatory wave propagation with velocities in the experimental range, using a relatively detailed description of the intracluster dynamics with a stochastic model of the IP_3R as the elementary unit. Nevertheless, this is only an example of the capabilities of the method. In order to advance onto a more detailed comparison with experimental data we would need a better

knowledge of various of the parameters that enter the model or replace the lack of knowledge with an exploration of the behaviors it supports for different parameter values. In this way, our approach could be used, for example, to explore in detail the results of Ref. [45], where it has been shown that Ca^{2+} oscillations occur stochastically and not as the result of a deterministic process.

We think that the model we introduced in this work provides a good framework that may lead to further work on local and global Ca^{2+} signals using detailed single IP_3R models as a building block. This kind of approach may contribute to get a comprehensive understanding of Ca^{2+} signals over a large range of time and spatial scales. In particular, the model could be used to analyze the behaviors that different IP_3R models would predict, contrasting them against experimental data on Ca^{2+} puffs and waves, such as puff latencies or the dependence of the wave speed on $[IP_3]$.

ACKNOWLEDGMENTS

We acknowledge useful conversations with Luciana Bruno. D.F. and S.P.D. are members of the Carrera del Investigador Científico (CONICET). This research was supported by UBA (Grant No. UBACyT X208), Grant No. PICT 17-21001 of ANPCyT (Argentina), Santa Fe Institute, and CONICET (Grant No. PIP 5131).

APPENDIX: STOCHASTIC IP_3R MODEL AND SIMULATION PROCEDURE

We use the stochastic IP_3R model introduced by De Young and Keizer [17], with its original parameter values. The model considers that the channel has 4 identical and independent subunits. Each subunit has two binding sites for Ca^{2+} (one activatory and one inhibitory) and one site for IP_3. Therefore each subunit has eight possible states, usually denoted S_{ijk} $(i,j,k=0,1)$ where $i=1$ indicates the presence of an IP_3 molecule bound to the channel, $j=1$ a Ca^{2+} ion bound to the activatory site and $k=1$ the binding of a Ca^{2+} ion to the inhibitory site. The open state of the subunit is S_{110} and a channel is considered to be open when at least three of the subunits are in the open state. Transitions between states are either constant or linearly dependent on $[Ca^{2+}]$ or $[IP_3]$ (we use the original parameters published in Ref. [17] and, unless explicitly noted, $[IP_3]=10\ \mu M$). In most simulations, $[IP_3]$ is constant, but $[Ca^{2+}]$ changes in time due to the coupled reaction-diffusion of Ca^{2+} released by nearby channels within the cluster. As described in the paper, the $[Ca^{2+}]$ distribution within the cluster is determined in two ways: we either use the simplified model (Sec. III) or the full reaction-diffusion model (Sec. II). In both cases, we simulate the stochastic transitions between states of the channel using a discrete time Markov Chain procedure. Within the framework of the simplified model, we use $dt=10^{-5}$ s. When $[Ca^{2+}]$ within the cluster is simulated using the full reaction diffusion model, the same time step is used to update the state of the channels.

In Sec. VI we use a step of $[IP_3]$ at $t=0$ representing the time at which IP_3 is photoreleased. In that case, the states of the IP_3R are initially chosen at random using the stationary probability distribution, i.e., the probability of being in each state at a given $[Ca^{2+}]$ and $[IP_3]=0$ which can be obtained analytically.

[1] M. J. Berridge, M. D. Bootman, and P. Lipp, Nature (London) **395**, 645 (1998).
[2] S. Swillens, G. Dupont, L. Combettes, and P. Champeil, Proc. Natl. Acad. Sci. U.S.A. **96**, 13750 (1999).
[3] J. Shuai, H. J. Rose, and I. Parker, Biophys. J. **91**, 4033 (2006).
[4] L. Bruno, G. Solovey, A. C. Ventura, S. Dargan, I. Parker, and S. Ponce Dawson (unpublished).
[5] Y. Yao, J. Choi, and I. Parker, J. Physiol. (London) **482**, 533 (1995).
[6] N. Callamaras and I. Parker, Cell Calcium **15**, 66 (1994).
[7] D. O. Mak and J. K. Foskett, J. Gen. Physiol. **109**, 571 (1997).
[8] J. W. Shuai and P. Jung, Proc. Natl. Acad. Sci. U.S.A. **100**, 506 (2003).
[9] I. Parker and Y. Yao, J. Physiol. (London) **491**, 663 (1996).
[10] M. Bootman, E. Niggli, M. Berridge, and P. Lipp, J. Physiol. (London) **499**, 307 (1997).
[11] X. P. Sun, N. Callamaras, J. S. Marchant, and I. Parker, J. Physiol. (London) **509**, 67 (1998).
[12] I. Parker and Y. Yao, Proc. R. Soc. London, Ser. B **246**, 269 (1991).
[13] I. Parker, J. Choi, and Y. Yao, Cell Calcium **20**, 105 (1996).
[14] N. Callamaras, J. S. Marchant, X. P. Sun, and I. Parker, J. Physiol. (London) **509**, 81 (1998).
[15] P. C. da Fonseca, S. A. Morris, E. P. Nerou, C. W. Taylor, and E. P. Morris, Proc. Natl. Acad. Sci. U.S.A. **100**, 3936 (2003).
[16] I. Bezprozvanny, J. Watras, and B. E. Ehrlich, Nature (London) **351**, 751 (1991).
[17] G. W. De Young and J. Keizer, Proc. Natl. Acad. Sci. U.S.A. **89**, 9895 (1992).
[18] S. Swillens, P. Champeil, L. Combettes, and G. Dupont, Cell Calcium **23**, 291 (1998).
[19] D. Fraiman and S. P. Dawson, Cell Calcium **35**, 403 (2004).
[20] J. K. Foskett, C. White, K. H. Cheung, and D. O. Mak, Physiol. Rev. **87**, 593 (2007).
[21] G. D. Smith, L. Dai, R. M. Miura, and A. Sherman, SIAM J. Appl. Math. **61**, 1816 (2001).
[22] K. Bentele and M. Falcke, Biophys. J. **93**, 2597 (2007).
[23] J. W. Shuai and I. Parker, Cell Calcium **37**, 283 (2005).
[24] S. P. Dawson, J. Keizer, and J. E. Pearson, Proc. Natl. Acad. Sci. U.S.A. **96**, 6060 (1999).
[25] J. W. Shuai and P. Jung, Biophys. J. **83**, 87 (2002).
[26] H. DeRemigio and G. D. Smith, Cell Calcium **38**, 73 (2005).
[27] L. Diambra and N. Guisoni, Cell Calcium **37**, 321 (2005).
[28] G. Ullah and P. Jung, Biophys. J. **90**, 3485 (2006).
[29] J. Shuai and P. Jung, New J. Phys. **5**, 132 (2003).
[30] R. Thul and M. Falcke, Biophys. J. **86**, 2660 (2004).
[31] M. Bar, M. Falcke, H. Levine, and L. S. Tsimring, Phys. Rev.

Lett. **84**, 5664 (2000).
[32] M. Falcke, L. Tsimring, and H. Levine, Phys. Rev. E **62**, 2636 (2000).
[33] M. Naraghi and E. Neher, J. Neurosci. **17**, 6961 (1997).
[34] G. D. Smith, Biophys. J. **71**, 3064 (1996).
[35] S. Rudiger, J. W. Shuai, W. Huisinga, C. Nagaiah, G. Warnecke, I. Parker, and M. Falcke, Biophys. J. **93**, 1847 (2007).
[36] H. J. Rose, S. Dargan, J. Shuai, and I. Parker, Biophys. J. **91**, 4024 (2006).
[37] S. L. Dargan, B. Schwaller, and I. Parker, J. Physiol. (London) **556**, 447 (2004).
[38] S. L. Dargan and I. Parker, J. Physiol. (London) **553**, 775 (2003).
[39] M. J. Berridge and G. Dupont, Curr. Opin. Cell Biol. **6**, 267 (1994).
[40] M. J. Berridge, J. Exp. Biol. **200**, 315 (1997).
[41] A. P. Thomas, G. S. Bird, G. Hajnoczky, L. D. Robb-Gaspers, and J. Putney, FASEB J. **10**, 1505 (1996).
[42] J. Marchant, N. Callamaras, and I. Parker, EMBO J. **18**, 5285 (1999).
[43] M. D. Bootman and M. J. Berridge, Curr. Biol. **6**, 855 (1996).
[44] H. Cheng, M. R. Lederer, W. J. Lederer, and M. B. Cannell, Am. J. Physiol. **270**, C148 (1996).
[45] A. Skupin, H. Kettenmann, U. Winkler, M. Wartenberg, H. Sauer, S. C. Tovey, C. W. Taylor, and M. Falcke, Biophys. J. **94**, 2404 (2008).
[46] J. Sneyd, K. Tsaneva-Atanasova, J. I. Bruce, S. V. Straub, D. R. Giovannucci, and D. I. Yule, Biophys. J. **85**, 1392 (2003).
[47] M. Falcke, Biophys. J. **84**, 28 (2003).
[48] M. Falcke, Biophys. J. **84**, 42 (2003).
[49] L. T. Izu, S. A. Means, J. N. Shadid, Y. Chen-Izu, and C. W. Balke, Biophys. J. **91**, 95 (2006).
[50] S. Means, A. J. Smith, J. Shepherd, J. Shadid, J. Fowler, R. J. Wojcikiewicz, T. Mazel, G. D. Smith, and B. S. Wilson, Biophys. J. **91**, 537 (2006).